ALBEDO ELECTRONS BETWEEN 12 and 1000 Mev

by

Martin H. Israel*

California Institute of Technology

Pasadena, California 91109

*Present address: Department of Physics, Washington University,

St. Louis, Missouri 63130

ABSTRACT

We measured the flux of splash albedo electrons near Fort Churchill, Manitoba, on 9 July 1967. A directional electron detector, consisting of a scintillation-counter telescope, a gas Čerenkov counter, and a spark chamber with lead plates, was flown on a balloon near 2 g/cm^2 atmospheric depth and pointed toward the nadir. We observed fluxes of 94 ± 16, 47 ± 11, 27 ± 9, and 2^{+4}_{-2} electrons/m^2 sec sr in the energy intervals 12-50, 50-100, 100-350, and 350-1000 Mev, respectively. We also observed return albedo electrons near Palestine, Texas, in a balloon flight near 5 g/cm^2 atmospheric depth on 7 April 1967. Between 25 and 65 Mev we find 60 ± 26 return-albedo-electrons/m^2 sec sr. At higher energies the observed flux of downward moving electrons is consistent with being atmospheric secondaries; we give 2σ upper limits to the return albedo flux of 22, 12, and 6 electrons/m^2 sec sr in the energy intervals of 65-131, 131-411, and 411-1149 Mev, respectively. These return albedo fluxes are significantly lower than corresponding fluxes previously reported by Verma but are consistent with results of a calculation by Bland. Comparison between our observations at Fort Churchill and those at Palestine indicate a significant contribution to the splash albedo flux from primary particles with rigidity below 4.5 GV.

INTRODUCTION

Primary cosmic ray nuclei entering the earth's atmosphere interact with air nuclei and produce numerous secondary particles. Some of these interaction products move upward and emerge from the atmosphere as "splash albedo". The electron component of the albedo comes primarily from the decay of pions produced in the interactions. The $\pi \rightarrow \mu \rightarrow e$ decay of charged pions gives electrons directly, while the photons from the decay of neutral pions initiate electromagnetic cascades. Those charged splash albedo particles with rigidities below the local geomagnetic cutoff cannot escape from the earth. They spiral along magnetic field lines and re-enter the atmosphere in the opposite hemisphere at a geomagnetic latitude nearly equal to the latitude where they originated. These particles constitute the "return albedo".

No detailed calculation of the intensity or spectrum of the albedo electrons has been published, and only a few observations are available. Bland [1965] has made a rough calculation to derive an upper limit to the intensity of return albedo electrons near 45° geomagnetic latitude. Verma [1967] measured the vertical splash and return albedo near Palestine, Texas for electrons between 10 and 1100 Mev. He used a counter telescope which measured energy loss and range of incident particles. Schmoker and Earl [1965] observed return albedo electrons between 50 and 150 Mev with a cloud chamber detector near Minneapolis and in Texas. At similar latitudes, McDonald and Webber [1959] observed fast splash albedo as particles moving backward through an energy-loss-Čerenkov detector. They attributed it to

electrons with range greater than 10 g/cm^2. No previous measurements of splash albedo electrons near Fort Churchill have been reported.

As part of a program to study cosmic ray electrons, we have measured the flux of splash albedo electrons between 12 and 1000 Mev near Fort Churchill, Manitoba, and return albedo electrons in the same energy interval near Palestine, Texas. The results of these measurements are reported in this paper. We also observed return albedo electrons with energy below 100 Mev near Fort Churchill. The high latitude return albedo measurements are complicated by the diurnal variation of the geomagnetic cutoff, and we postpone presentation of these results to an accompanying paper [Israel and Vogt, 1969], hereinafter referred to as paper 2, in which we present observations of the diurnal variation.

INSTRUMENT

a) Detector system

Figure 1 shows a cross-section of our detector system. A triple coincidence of Telescope Counter 1 (T1), Telescope Counter 2 (T2), and the Gas Čerenkov Counter (C), triggers the electronic system which records the event. The scintillation counters, T1 and T2, define an acceptance cone with a geometrical factor of 0.90 ± 0.02 cm^2 sr. The maximum opening angle is 13.2° from the axis.

The Čerenkov counter is filled with sulfur hexafluoride at 2.2 atmospheres absolute pressure (at 25°C), which gives a velocity threshold of 0.9984 c, corresponding to a kinetic energy of 8.6 Mev for electrons and 15.8 Gev for protons.

The pulse heights from the scintillation counters Energy Loss 1 and Energy Loss 2 (ΔE1 and ΔE2) are recorded for each event. Pulse height in ΔE1 corresponding to minimum energy loss establishes that one, singly charged particle traversed the telescope. The counter ΔE2 samples the electron shower independently of the spark chamber.

A high voltage pulse is applied to the spark chamber plates at each T1, T2, C triple coincidence, and the position of each spark is recorded digitally. A lead plate with a thickness of 11.6 g/cm^2 (2 radiation lengths) is above the chamber, and three lead plates, each 5.8 g/cm^2 thick, are inside the chamber; a pair of chamber gaps is below each lead plate.

The chamber shows no sparks for electrons stopping in the first lead plate, indicating their short range. For more energetic electrons, the chamber indicates the development of their cascade shower. These electrons can be

distinguished from the protons which penetrate the lead without a nuclear interaction, because the latter leave a single straight track in the spark chamber.

Most protons which do interact in the detector are eliminated by the guard counters. These counters completely surround the chamber, except for apertures for the allowed particle beam. For each event we record whether a guard counter is triggered in coincidence with the telescope counter. An interacting 16 Gev proton has greater than 90 percent probability of sending at least one charged particle through a guard counter [Israel, 1969a]. The guard counters also allow us to eliminate charged particles which enter the detector from outside the acceptance cone, but give a triple coincidence by interacting in the lead and sending particles up through the telescope counters.

b) Electronic system

After each event, two types of data are recorded digitally on magnetic tape.

(1) Data describing this event.
   (a) Pulse heights from ΔE1 and ΔE2.
   (b) One bit indicating a T1, T2, C triple coincidence.
   (c) Three guard bits; one indicating output from the top guard counter, another indicating any of the side guards, the third for the bottom guard.
   (d) The position of each spark in the chamber.

(2) Related information.
   (a) Accumulated count of single pulses from the guard counters.
   (b) Accumulated count of single pulses from the Čerenkov counter.

(c) Accumulated count of T1, T2 double coincidences.

(d) Temperature.

(e) Time.

Figure 2 is a general block diagram of the electronic system. A triple coincidence among T1, T2, and C, triggers the high voltage pulser, which applies 8 kv to the spark chamber. The primary coincidence also activates the control logic and produces one of the inputs to the guard coincidence logic. The busy signal from the control logic blocks the coincidence, preventing any further events from triggering the system until this event has been recorded on the magnetic tape. The control logic also opens the linear gate on the input of each pulse height analyzer permitting the analysis of the ΔE1 and ΔE2 outputs. Then the control transfers all the data, except the spark information, through the output buffers onto the magnetic tape. Finally it interrogates the cores and writes the position of each spark onto the tape.

c) Spark chamber

Each gap of the chamber is a self-contained module consisting of a high-voltage plane, Lucite spacer, ground plane, and core board (Fig. 3). The planes and spacer together form an enclosure for the chamber gas. The gas is 90 percent neon and 10 percent helium. The gap width is 0.64 cm and the sensitive area of each gap is 10 cm square.

The chamber readout is digitized with ferrite memory cores. The ground plane of each gap consists of ninety-six parallel copper strips with 1 mm spacing on a glass-epoxy board. Each strip extends out of the gap and connects to a wire which passes through a memory core before being connected to ground. When a spark strikes a strip, the spark current passes through the core and reverses the magnetization direction of the core. After the

spark noise dies away, the cores are interrogated and reset to their normal state. The position of each set core is recorded on magnetic tape, indicating the positions of the sparks. Alternate gaps of the spark chamber have ground strips oriented at right angles to one another, giving two orthogonal views of each event.

The high-voltage plane is a sheet of 0.16 cm aluminum covered on the inside with a 0.04 cm layer of nylon. The important effect of the nylon is the reduction of spark spreading. With the nylon covering the aluminum, approximately 90 percent of all sparks set only one core, and the remaining 10 percent set two adjacent cores. Fewer than 0.1 percent set three adjacent cores. This enables us to resolve two sparks 0.2 cm apart.

The 8 kv high-voltage pulse is applied to the chamber by two sealed spark gaps (EG+G, GP17A). Each spark gap drives four of the chamber modules. The spark gaps are triggered by a 5 kv pulse from a krytron, which is in turn triggered by an avalanche transistor and pulse transformer. The electronic delay from the output of the photomultipliers to the appearance of the high voltage on the spark chamber is 140 ± 20 nsec.

An aluminum box completely surrounds the spark chamber. It shields the photomultipliers, discriminators, pulse height analyzers, and associated circuits from the radio frequency noise of the sparks.

BALLOON FLIGHTS

The data reported in this paper are derived from two balloon flights of our electron detector. In a flight launched at Fort Churchill, Manitoba, on 9 July 1967, the detector system was pointed toward the nadir to observe the splash albedo. The balloon floated for 10.4 hours at an atmospheric depth of 2.3 g/cm^2.

A flight with the instrument oriented toward the zenith was launched at Palestine, Texas, on 7 April 1967 and floated at 5.2 g/cm^2 for six hours. Throughout the flight the vertical geomagnetic cutoff rigidity at the location of the detector remained above 3.8 GV. [Shea, et al, 1968]. The electrons which we observed were all well below cutoff and so consist of atmospheric secondaries produced above the detector and return albedo, but no primaries. The data from this flight are not optimal because of a balloon failure which resulted in the detector floating at 5.2 g/cm^2 instead of the expected 2 g/cm^2. This lower altitude gave a larger flux of atmospheric secondaries than desired.

DATA ANALYSIS

a) Event selection and energy determination

We attribute to electrons those recorded events satisfying the following four criteria:

(1) A triple coincidence, including the Čerenkov counter, is registered.

(2) No guard counter signal accompanies the event.

(3) The pulse height from the counter $\Delta E1$ corresponds to energy loss between 0.5 I_o and 1.7 I_o, where I_o is the most probable energy loss of a relativistic singly charged particle.

(4) Either (a) there is no output from $\Delta E2$,

or (b) there is an output from $\Delta E2$ corresponding to energy loss greater than 1.7 I_o, and the spark chamber did not show a single straight track.

These criteria eliminate most of the background due to particles other than electrons, but they also eliminate some electrons. The solid curve in Figure 4 shows the electron detection efficiency as a function of energy.

For electrons with energy between 100 Mev and 1000 Mev we determined the efficiency directly, using the monoenergetic external electron beam at the California Institute of Technology synchrotron. At these energies, the rejection of electrons is principally due to the second criterion - guard counter signals. For lower energies, we derive the efficiency from a combination of measurements and calculations. Below 30 Mev the detection efficiency curve is dominated by the calculated Čerenkov counter response. We estimate that systematic uncertainties in the detection efficiency produce errors of less than 10 percent of the observed flux at all energies considered.

We divide the selected events into four categories.

Type 1: Both the spark chamber and ΔE2 register no particle.

Type 2: ΔE2 registers no particle and the total number of sparks in all chamber gaps is one, two, or three.

Type 3: ΔE2 registers no particle, and the total number of sparks is greater than three.

Type 4: ΔE2 registers a pulse height corresponding to energy loss greater than 1.7 I_o.

These four types correspond approximately to electron energies at the top of the detector of 12 to 50, 50 to 100, 100 to 350, and 350 to 1000 Mev respectively. We calibrated the detector using the monoenergetic external electron beam of the Caltech synchrotron to determine the energy dependence

of the probability for producing each type of event. We derive an electron spectrum from the observed number of events of each type with the following iterative unfolding technique. We make a first estimate of the differential energy spectrum, j(E). From calibration of the detector we have curves for the probability, $p_i(E)$, that an electron of energy E be detected as an event of type i. We then calculate the fraction, f_{ik}, of events of type i due to electrons with energy between E_k and E_{k+1} as:

$$f_{ik} = \frac{\int_{E_k}^{E_{k+1}} p_i(E)\, j(E)\, dE}{\int_{E_k}^{E_{k+1}} j(E)\, dE} \qquad (1)$$

The number, N_k, of incident electrons in the k^{th} energy interval is calculated from the number, n_i, of observed events of type i by

$$N_k = \frac{1}{\eta_k} \sum_{i=1}^{4} n_i \, f_{ik} \qquad (2)$$

where η_k is the detection efficiency in the k^{th} energy interval. If the detection efficiency curve of Fig. 4 is $\eta(E)$, then

$$\eta_k = \frac{\int_{E_k}^{E_{k+1}} \eta(E)\, j(E)\, dE}{\int_{E_k}^{E_{k+1}} j(E)\, dE} \qquad (3)$$

From the N_k we calculate an electron spectrum. If this spectrum does not agree with the spectrum originally assumed, we repeat the previous steps using this newly calculated spectrum as the assumed spectrum. We continue this iterative procedure until the calculated spectrum differs from the assumed spectrum by less than the statistical uncertainty. Usually the process converges after one or two iterations.

b) Systematic uncertainties

Possible differences between the spark chamber efficiency during flight and during the calibration at the Caltech synchrotron result in a possible error of $\pm$ 7 percent in the electron flux between 100 and 350 Mev. In other energy intervals the error from this source is less than 3 percent.

An additional uncertainty occurs because we could not measure the detection efficiency for electrons above 1 Gev. Thus an undetermined fraction of the type 4 events is due to these higher energy electrons. This fraction is small because of the steepness of the differential electron spectrum. Even for a relatively flat spectrum, proportional to E^{-1} (where E is electron energy), the uncertainty in the flux between 350 and 1000 Mev would be less than 15 percent.

We have considered in detail the possibility of contamination of our electron measurements by protons, pions, and muons [Israel, 1969a]. The only serious source of error is protons with energy above the gas Čerenkov counter threshold (16 Gev) which interact in the detector system. For the flight from Texas with the detector pointed toward the zenith, an upper limit to the proton contamination is 40 percent of the flux of 350-1000 Mev electrons. (This uncertainty is comparable to the statistical uncertainty because we

observed only 4 events in this energy interval.) For the flight in which the detector was oriented toward the nadir, the contamination is negligible.

c) Correction for atmospheric secondaries

The analysis described above permits us to calculate the spectrum of electrons incident on the detector system. For the flight in which the detector looked at the zenith, the quantity of physical interest is the electron flux incident at the top of the atmosphere. We must, therefore, subtract the contribution of atmospheric secondary electrons from the observed spectrum.

We use the spectrum of atmospheric secondary electrons arising from the interaction of primary cosmic ray nuclei with air nuclei which has been calculated by Perola and Scarsi [1966]. We correct their results by the addition of knock-on electrons [K. P. Beuermann, to be published], which are significant below 30 Mev. Justification for this method of correcting for secondaries is given in an accompanying paper [Israel, 1969b], hereinafter referred to as paper 3, in which our experimental depth dependence of observed low-energy electrons is compared with the calculations.

RESULTS

a) Splash albedo electrons near Fort Churchill

During the flight of 9 July 1967 we observed electrons moving vertically upward. Fig. 5 displays the altitude dependence of the rate of type 1 events and of types 2 and 3. The data points at 2.3 g/cm^2 atmospheric depth represent averages over the 10.4 hour float period. The other data were gathered during the 5.6 hour ascent.

It is apparent from Figure 5 that there is little or no altitude variation of the splash albedo between 2.3 g/cm^2 and 50 or 100 g/cm^2. We shall therefore assume that the electron energy spectrum which we observe at the detector at 2.3 g/cm^2 is the same as the spectrum at the top of the atmosphere. The number of events of each type observed during the float period of flight C3 is shown in Table 1. Applying the analysis described above, we derive the flux values shown in Table 2. The solid circles in Figure 6 indicate the differential energy spectrum derived from these measurements. The error limits quoted include statistical and systematic uncertainties.

To simplify comparison between our results and those of other experimenters, Table 2 gives our fluxes summed over various energy intervals. In Table 3 we summarize the splash albedo results of other observers. We note that in all energy intervals our measured flux lies significantly below that quoted by Verma. On the other hand, our flux above 50 Mev is in reasonable agreement with that of McDonald and Webber, and our flux above 100 Mev is consistent with the upper limit derived by Deney et al.

b) Return albedo near Palestine, Texas

The number of events of each type observed during the float period of the 7 April flight is listed in Table 1. In Table 4, line 2, we present the electron fluxes in various energy intervals derived from these events. The corresponding differential energy spectrum is plotted as solid points in Figure 7. Also shown, in line 3 of Table 4, is the flux of atmospheric secondary electrons expected at 5 g/cm^2 near Palestine. The only energy interval in which we observe a clear excess over the secondaries is 12 to 50 Mev where the return albedo contribution is 60 $\pm$ 26 electrons/m^2 sec sr. For the other intervals, line 5 of Table 4 gives upper limits to the return

albedo contribution. These limits represent two standard deviations of statistical uncertainties, plus the systematic uncertainty.

For comparison between the return and splash albedo it is necessary to take account of the energy loss of the return albedo electrons between the top of the atmosphere and the detector. Using calculated values of electron range in air, including energy loss by both ionization and radiation [Berger and Seltzer, 1964], we derived the tabulated energy intervals at the top of the atmosphere. In the last line of Table 4 we list the splash albedo fluxes from the Fort Churchill flight in these higher energy intervals. We derived these flux values from those of Table 2 using the observed differential splash albedo spectrum from Figure 6.

For further comparison, Table 5 lists results from return albedo measurements by other observers. We have tabulated the total observed flux, including return albedo and atmospheric secondaries. These results are also plotted in Figure 7. Again we note a significant disagreement between our results and those of Verma.

DISCUSSION

We first compare our return albedo measurement near Palestine, Texas, with Verma's. His measurements were made on two balloon flights also launched at Palestine. Since the flux of atmospheric secondaries at the float altitude of his flights (4.0 g/cm^2) is within 25 percent of that at the altitude of our flight (5.2 g/cm^2), we shall compare the total observed fluxes; i.e., return albedo plus atmospheric secondaries.

The two year time difference between Verma's flights and ours can account for only a small part of the difference in results. From 1965, when his data were taken, to the time of our flights the Mt. Washington neutron monitor count rate decreased by 9 percent. The corresponding decrease in the flux of cosmic ray protons and helium nuclei above the geomagnetic cutoff at Palestine (4.5 GV) is 10 percent. (This number is based upon regression curves of data from the last solar cycle, [Webber, 1967]). The corresponding decrease in the albedo intensity must be $\leq$10 percent. This upper limit follows because the change in primary flux is largest at the lowest energy while the electron production by electromagnetic cascades is larger at higher primary energies. Similarly, the change in flux of atmospheric secondaries must be $\leq$10 percent. A 10 percent reduction in Verma's flux between 10 and 100 Mev would bring it within the quoted error of our result. For energies above 100 Mev, however, the difference between his results and ours remains significant.

This difference indicates the possibility of a systematic error in either Verma's or our measurements. A conceivable source of error in our results could lie in the determination of our detection efficiency (Fig. 4). In particular, the guard counters surrounding our spark chamber eliminate those incident electrons which cause a shower that escapes the lead stack and triggers a guard counter. We are satisfied that there is no significant error in our determination of the probability of such a shower. We measured this probability, as a function of energy, at the Caltech synchrotron both before and after our flights and obtained consistent results. Furthermore, in the energy interval between 350 and 1000 Mev, our return albedo flux is at least

a factor of four below Verma's, while in the same energy interval, our primary flux measurements at Churchill in 1967 are less than a factor of two below published measurements for 1966; and this factor may be due to modulation (see paper 3).

We may also compare our return albedo measurement with the results of Bland [1965]. He has published a rough calculation of the return albedo flux at 4 g/cm^2 atmospheric depth, 45° geomagnetic latitude. His result, as an upper limit to the flux of electrons above 100 Mev, is 14 electrons/m^2 sec. If the electrons are isotropic over the upper hemisphere, this would correspond to 2.2 electrons/m^2 sec sr. This flux is consistent with our upper limit, 18 electrons/m^2 sec sr after subtracting atmospheric secondaries. Verma, on the other hand, derives a corresponding value of 94 $\pm$ 25 electrons/m^2 sec sr.

We next consider our measurement of the splash albedo near Fort Churchill. Both the location and the time of the measurement by McDonald and Webber near Minneapolis enable us to compare their result with ours. The geomagnetic cutoff at Minneapolis, 1.4 GV, corresponds to a proton energy of 750 Mev. The difference between this cutoff and that near Churchill, $\lesssim$100 MV, is not significant for the production of albedo electrons. At the time of the Minneapolis flight, the Mt. Washington neutron monitor count rate was 2302, 0.7 percent higher than during our flight. This corresponds to a 6 percent difference in the primary proton flux [Webber, 1967] and less than 6 percent in the albedo flux. The albedo flux measured by McDonald and Webber, 84 $\pm$ 8 electrons/m^2 sec sr, is in good agreement with our corresponding flux, 76 $\pm$ 17 electrons/m^2 sec sr, above 50 Mev.

We cannot attempt to draw any conclusion about the latitude dependence of the splash albedo from comparison of our results with Verma's because of the instrumental differences previously noted. We shall, however, compare our own return albedo measurement near Palestine with our splash albedo observation near Churchill (lines 4-7 of Table 4). It would be preferable to compare splash albedo measurements with the same detector at the two locations; however, technical difficulties prevented us from making splash albedo measurements near Palestine.

The intensities of the splash and the return albedo at rigidities below the local geomagnetic cutoff are expected to be equal at any point at the top of the atmosphere, provided that the magnetic field strength at the given point is the same as at the conjugate point in the other hemisphere. This equality follows from the splash origin of the return albedo and the fact that the primary cosmic ray flux at a given geomagnetic latitude in the northern and southern hemispheres is the same. However, although the splash and return intensities, integrated over all directions, should be the same, the vertical splash albedo flux may be lower than the vertical return albedo flux. The dominant source of splash albedo electrons is likely to be cascade showers from interactions of primary cosmic rays which enter the atmosphere at grazing incidence [Bland, 1965]. Such showers tend to be collimated in the direction of the incident primary particle, so we expect the splash albedo to be most intense at large zenith angles. Treiman [1953] has pointed out that the return albedo will tend to be less anisotropic than the splash albedo. As a result, we expect the vertical return albedo flux to be an upper limit to the vertical splash albedo, at the same location.

We note that this expected relationship between the splash and return albedo fluxes has not been extensively tested. The only previously published observation of both splash and return albedo electrons with the same instrument near the same location is that of Verma [1967]. The observed difference between the splash and return albedo fluxes was not considered significant. Also, we show in paper 2 that our observations near Fort Churchill are consistent with equality between the splash and return albedo fluxes below 100 Mev. However, we feel that uncertainty in the precise value of the "daytime" geomagnetic cutoff at the location of the detector introduces significant uncertainty in the interpretation of any return albedo measurement near Fort Churchill.

For the purpose of discussing our results (Table 4) we assume that the return albedo flux which we observed near Palestine is indeed an upper limit to the splash albedo flux at the same location. Between 65 and 131 Mev, the Churchill splash albedo exceeds the Palestine return albedo by at least 50 percent, while between 25 and 65 Mev the return and splash albedo fluxes are in agreement. We cannot explain the apparent difference between these two adjacent energy intervals; however, we note that our results are consistent with a 50 percent flux excess at Churchill over the entire observed energy interval. Such an excess at Churchill indicates that primary cosmic rays below the 4.5 GV cutoff of Palestine contribute significantly to the production of splash albedo electrons. Since the flux of primaries below 4.5 GV displays significant modulation over the solar cycle, we expect that the splash albedo electron flux at high latitudes will exhibit similar long-term variations.

Acknowledgements

I am most grateful to Professor Rochus Vogt who suggested this research project and offered valuable guidance and support throughout its execution. It is also a pleasure to acknowledge stimulating discussions with Dr. Klaus Beuermann, and Professor Edward Stone.

This research was carried out under NASA grant NGL-05-002-007.

TABLE 1

NUMBER OF ELECTRON EVENTS OBSERVED

Flight date	9 July 1967	7 April 1967
Launch location	Fort Churchill	Palestine
Detector orientation	nadir	zenith
Event type 1	212	152
2	86	42
3	21	15
4	3	5
Sensitive time (min)	496	346

TABLE 2

SPLASH ALBEDO ELECTRONS

RESULTS OF THIS EXPERIMENT - FORT CHURCHILL, MANITOBA

Energy interval (Mev)	12 - 50	50 - 100	100 - 350	350 - 1000
Flux (electrons/m^2 sec sr)	94 ± 16	47 ± 11	27 ± 9	2^{+4}_{-2}
Combined flux, 12 - 100 Mev and 100 - 1000 Mev		141 ± 24		29 ± 10
Flux between 50 and 1000 Mev			76 ± 16	

TABLE 3

SPLASH ALBEDO ELECTRONS

RESULTS OF OTHER EXPERIMENTS

Ref.	Date	Location	Cutoff[a] (GV)	Energy Interval (Mev)	Flux (electrons/m^2 sec sr)
Verma, 1967	1965	Palestine, Texas	4.5	10 - 100	467 ± 48
				100 - 300	134 ± 15
				300 - 1100	108 ± 18
McDonald and	1956	Iowa City	1.8	$\gtrsim$ 40[b]	84 ± 8
Webber, 1959	1956	Minneapolis	1.4	$\gtrsim$ 40[b]	89 ± 8
Deney et al 1968	1967	Palestine, Texas	4.5	> 100	< 100

(a) Shea et al [1968]

(b) These electrons were identified only as having range greater than 10 g/cm^2. The corresponding energy is estimated from our own detector calibration at the Caltech synchrotron.

TABLE 4

RETURN ALBEDO - THIS EXPERIMENT - PALESTINE, TEXAS

(fluxes in units of electrons/m^2 sec sr)

1.	Energy interval at detector (Mev)	12 - 50	50 - 100	100 - 350	350 - 1000
2.	Total observed flux at 5.2 g/cm^2	95 ± 19	29 ± 9	31 ± 14	$8\ ^{+8}_{-4}$
3.	Calculated flux of atmospheric secondaries	35 ± 7	26 ± 5	50 ± 10	17 ± 3
4.	Return albedo flux	60 ± 26			
5.	Return albedo flux upper limit (2σ)	(96)	22	12	6
6.	Energy interval at the top of the atmosphere (Mev)	25 - 65	65 - 131	131 - 411	411 - 1149
7.	Corresponding splash albedo flux, near Fort Churchill.	63 ± 11	44 ± 10	13 ± 4	5

TABLE 5

RETURN ALBEDO - OTHER EXPERIMENTS

Ref.	Date	Location	Cutoff (GV)	Atmospheric depth (g/cm^2)	Energy Interval (Mev)	Total observed flux at detector (electrons/m^2 sec sr)
Verma, 1967a	1965	Palestine, Texas	4.5	4.0	10 - 100	162 ± 16
					100 - 300	90 ± 30
					300 - 1100	68 ± 10
Schmoker and Earl, 1965	1962	San Angelo, Texas	5.0	6	45 - 150	140 ± 70
	1962 and 63	Minneapolis	1.4	4 - 5	45 - 150	180 ± 60

REFERENCES

Bland, C. J., An estimate of the contribution from reentrant albedo to the measurement of primary electrons, Space Research V, ed. D. G. King-Hele, 618, North Holland Publishing Co., Amsterdam, 1965.

Deney, C. L., M. F. Kaplan, and P. W. Lommen, Integral fluxes of primary cosmic rays at Palestine, Texas, and Fort Churchill, Canada, near solar minimum (abstract), Bull. Am. Phys. Soc. 13, 63, 1968.

Israel, M. H., Primary cosmic ray electrons and albedo electrons in 1967 at energies between 12 and 1000 Mev, Ph. D. Thesis, California Institute of Technology, Pasadena, 1969a.

Israel, M. H., Primary cosmic ray electrons in 1967 between 17 and 1000 Mev, J. Geophys. Res. 74, 1969b. (accompanying paper)

Israel, M. H. and R. E. Vogt, Diurnal intensity variation of low-energy electrons near Fort Churchill, Canada, during 1967, J. Geophys. Res. 74, 1969. (accompanying paper)

McDonald, F. B. and W. R. Webber, Proton component of the primary cosmic radiation, Phys. Rev. 115, 194, 1959.

Perola, G. C. and L. Scarsi, Flux and energy spectrum of secondary electrons in the upper atmosphere, Nuovo Cimento 46, 718, 1966.

Schmoker, J. W. and J. A. Earl, Magnetic-cloud-chamber observations of low-energy cosmic-ray electrons, Phys. Rev. 138, B300, 1965.

Shea, M. A., D. F. Smart, and J. R. McCall, A five degree by fifteen degree world grid of trajectory-determined vertical cutoff rigidities, Can. J. Phys. 46, S1098, 1968.

Treiman, S. B., The cosmic-ray albedo, Phys. Rev. 91, 957, 1953.

Verma, S. D., Measurement of the charged splash and re-entrant albedo of the cosmic radiation, J. Geophys. Res. 72, 915, 1967.

Webber, W. R., The spectrum and charge composition of the primary cosmic radiation, Handbuch der Physik, Vol. 46, part 2, ed. K. Sitte, 181, Springer-Verlag, Berlin, 1967.

FIGURE CAPTIONS

Fig. 1 Cross-section of the detector system

Fig. 2 Electronic block diagram

DISC - discriminator

CSA - charge sensitive amplifier

PHA - pulse height analyzer

Dashed line indicates components enclosed by spark noise shield.

Fig. 3 Exploded view of one chamber module

Fig. 4 Electron detection efficiency vs. kinetic energy at the top of the detector.

Solid curve - efficiency with all selection criteria included

Dashed curve - efficiency with fourth criterion ignored.

Fig. 5 Event rate of upward moving electrons vs. atmospheric depth.

Solid circles - type 1 events

Open circles - type 2 and 3 events

Fig. 6 Differential kinetic energy spectrum of splash albedo electrons.

Solid circles - present experiment, Fort Churchill, Canada

Open circles - Verma [1967], Palestine, Texas

Fig. 7 Differential kinetic energy spectrum of downward moving electrons below geomagnetic cutoff. Data points indicate total observed flux, including return albedo and atmospheric secondaries. Solid curve indicates calculated spectrum of atmospheric secondaries at 5 g/cm^2 atmospheric depth. Dashed curves indicate quoted uncertainty in this calculated spectrum ($\pm$ 20 °/o).

Solid circles - present experiment, Palestine, Texas, 5 g/cm^2.

Open circles - Verma [1967], Palestine, Texas, 4 g/cm^2

Solid line diamond - Schmoker and Earl [1965], San Angelo, Texas, 6 g/cm^2.

Dashed line diamond - Schmoker and Earl [1965], Minneapolis, Minn., 4-5 g/cm^2.

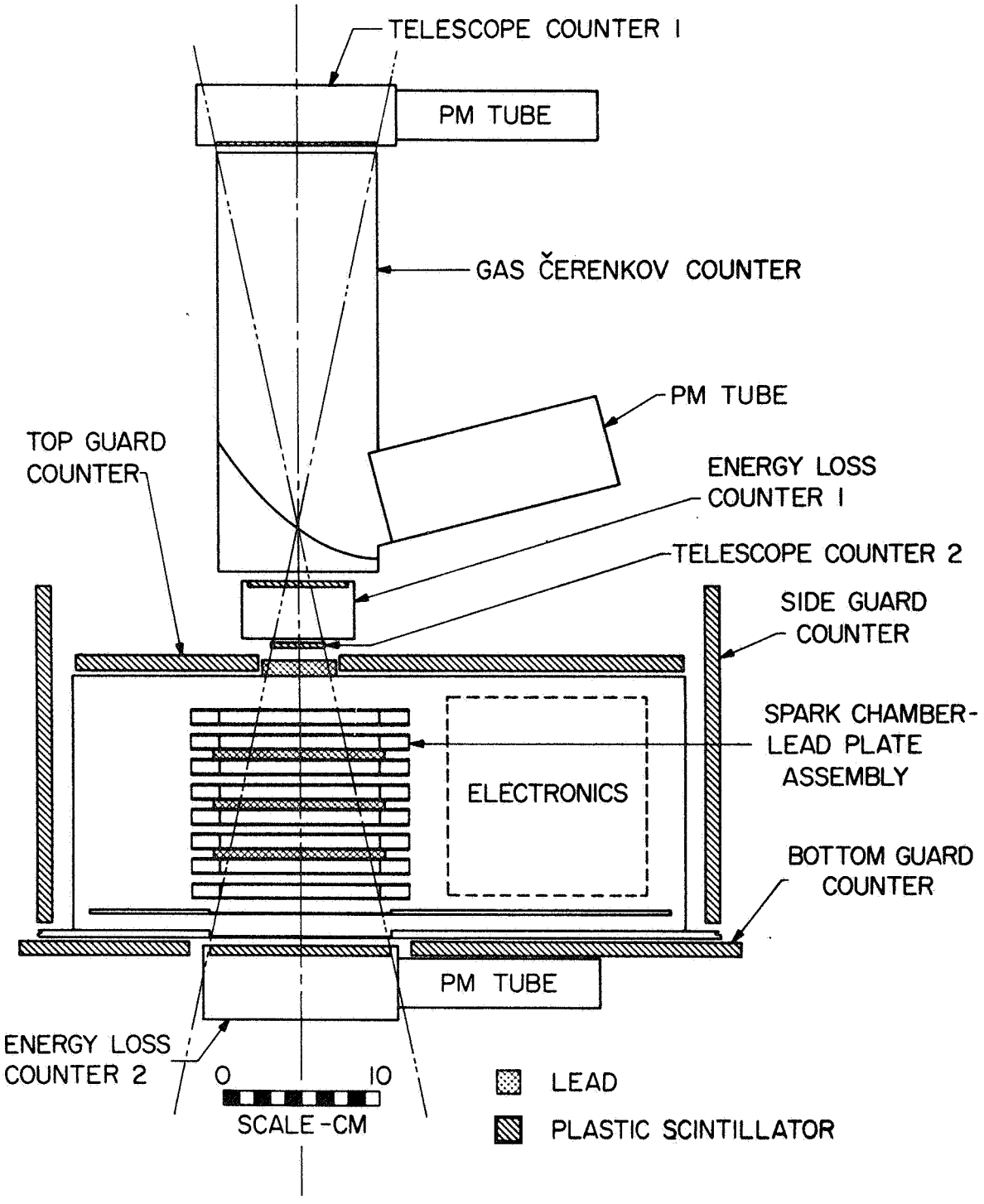
TELESCOPE COUNTER I
PM TUBE
GAS ČERENKOV COUNTER
PM TUBE
TOP GUARD COUNTER
ENERGY LOSS COUNTER I
TELESCOPE COUNTER 2
SIDE GUARD COUNTER
SPARK CHAMBER-LEAD PLATE ASSEMBLY
ELECTRONICS
BOTTOM GUARD COUNTER
PM TUBE
ENERGY LOSS COUNTER 2
0
10
SCALE-CM
LEAD
PLASTIC SCINTILLATOR

Figure 1

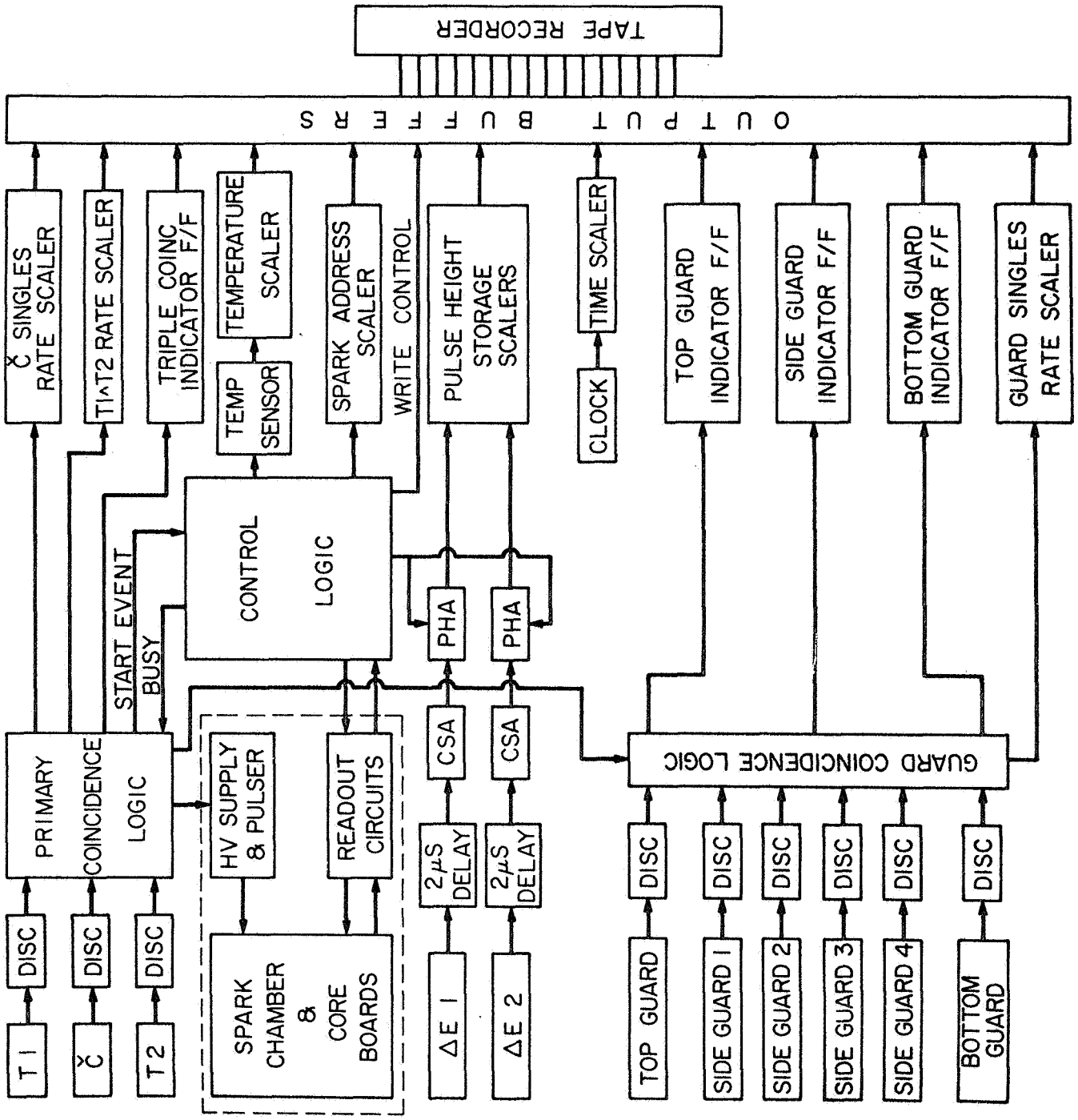
TAPE RECORDER
OUTPUT BUFFERS
Č SINGLES RATE SCALER
T1^T2 RATE SCALER
TRIPLE COINC INDICATOR F/F
TEMPERATURE SCALER
TEMP SENSOR
SPARK ADDRESS SCALER
WRITE CONTROL
PULSE HEIGHT STORAGE SCALERS
TIME SCALER
CLOCK
TOP GUARD INDICATOR F/F
SIDE GUARD INDICATOR F/F
BOTTOM GUARD INDICATOR F/F
GUARD SINGLES RATE SCALER
CONTROL LOGIC
START EVENT
BUSY
PHA
PHA
PRIMARY COINCIDENCE LOGIC
HV SUPPLY & PULSER
READOUT CIRCUITS
CSA
CSA
2μS DELAY
2μS DELAY
GUARD COINCIDENCE LOGIC
DISC
DISC
DISC
DISC
DISC
DISC
DISC
DISC
T1
Č
T2
SPARK CHAMBER & CORE BOARDS
ΔE 1
ΔE 2
TOP GUARD
SIDE GUARD 1
SIDE GUARD 2
SIDE GUARD 3
SIDE GUARD 4
BOTTOM GUARD

Figure 2

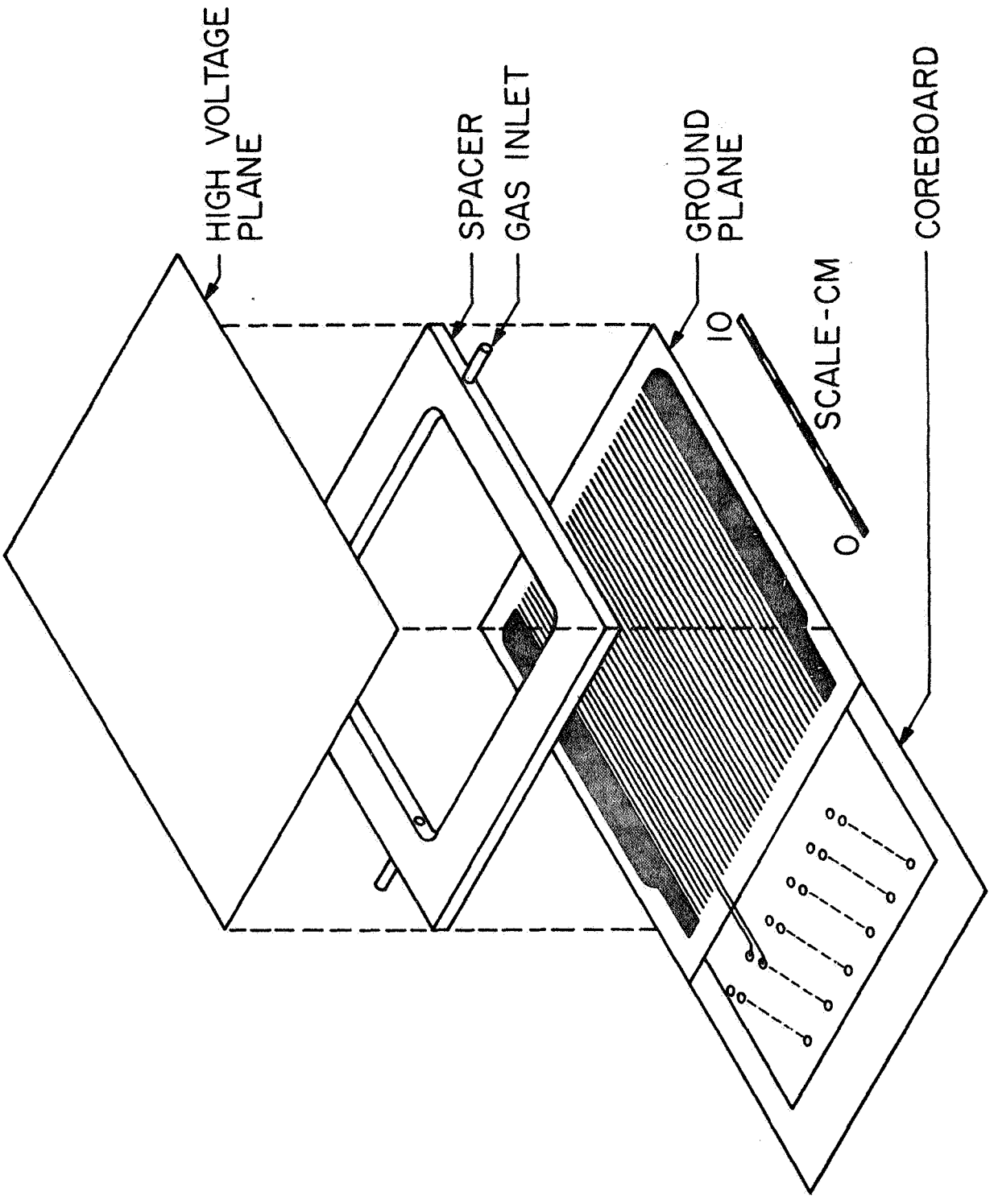
HIGH VOLTAGE PLANE
SPACER
GAS INLET
GROUND PLANE
COREBOARD
0
10
SCALE-CM

Figure 3

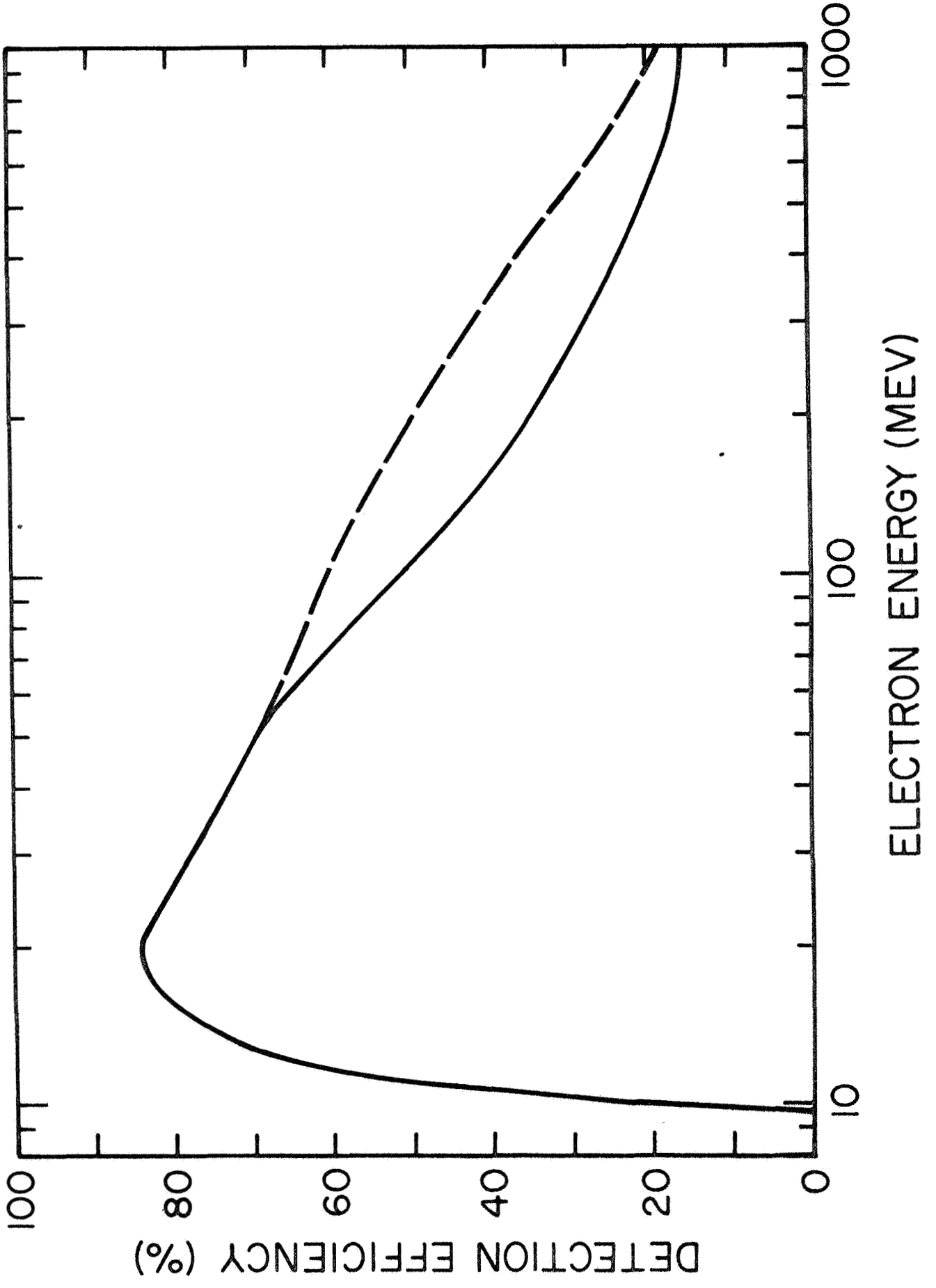
DETECTION EFFICIENCY (%)
100
80
60
40
20
0
10
100
1000
ELECTRON ENERGY (MEV)

Figure 4

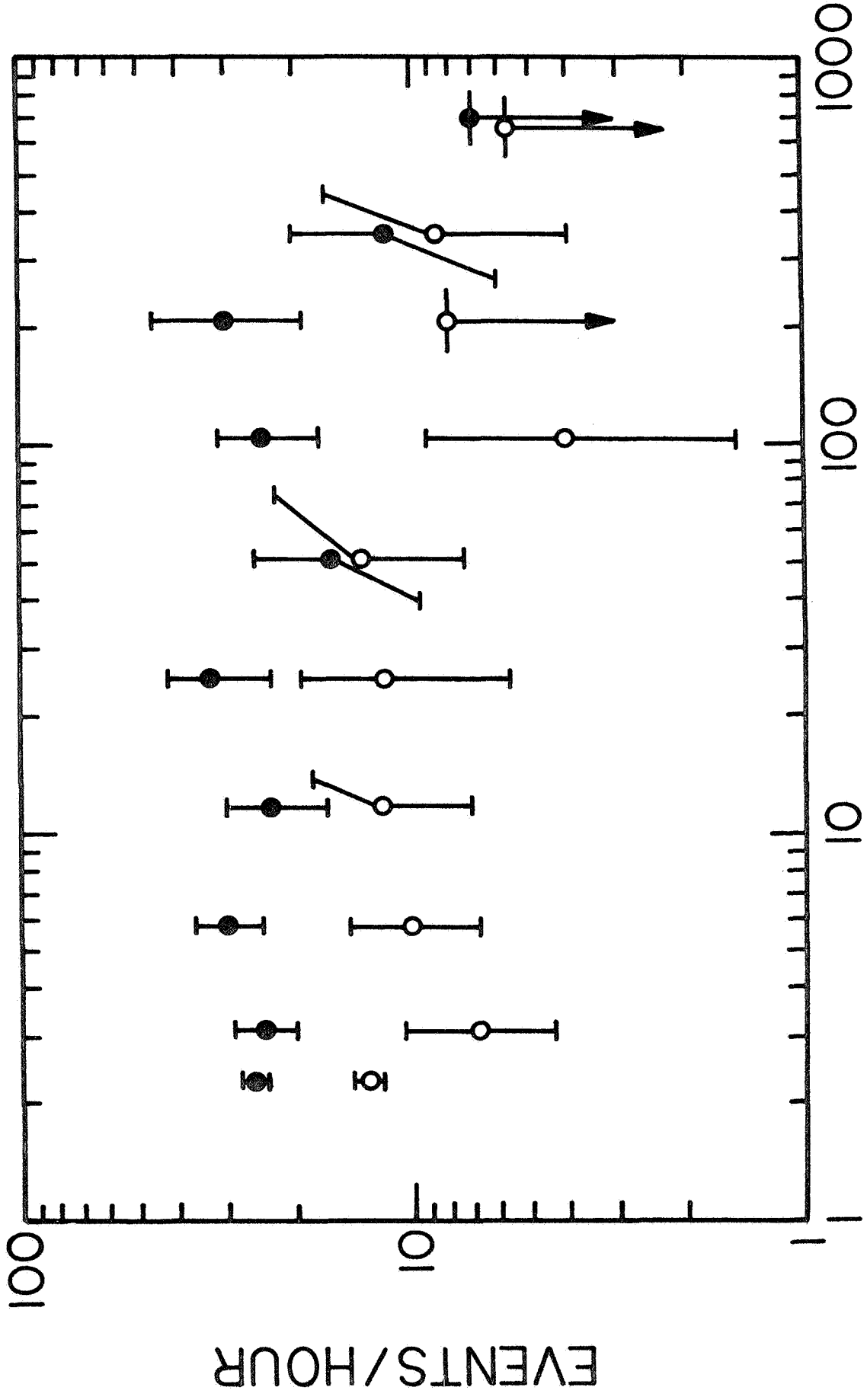

Figure 5

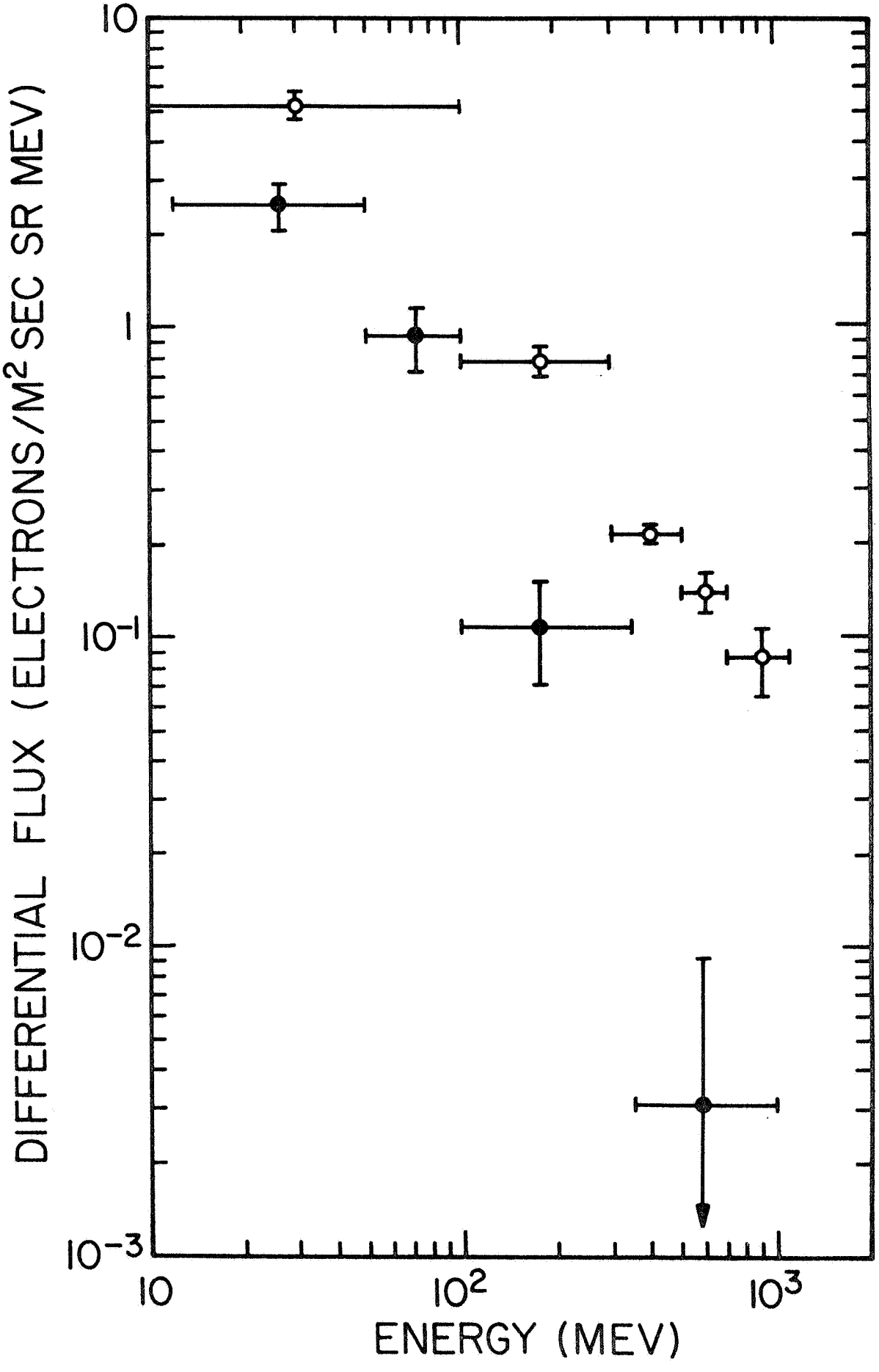
DIFFERENTIAL FLUX (ELECTRONS/M² SEC SR MEV)
10
1
10⁻¹
10⁻²
10⁻³
10
10²
10³
ENERGY (MEV)

Figure 6

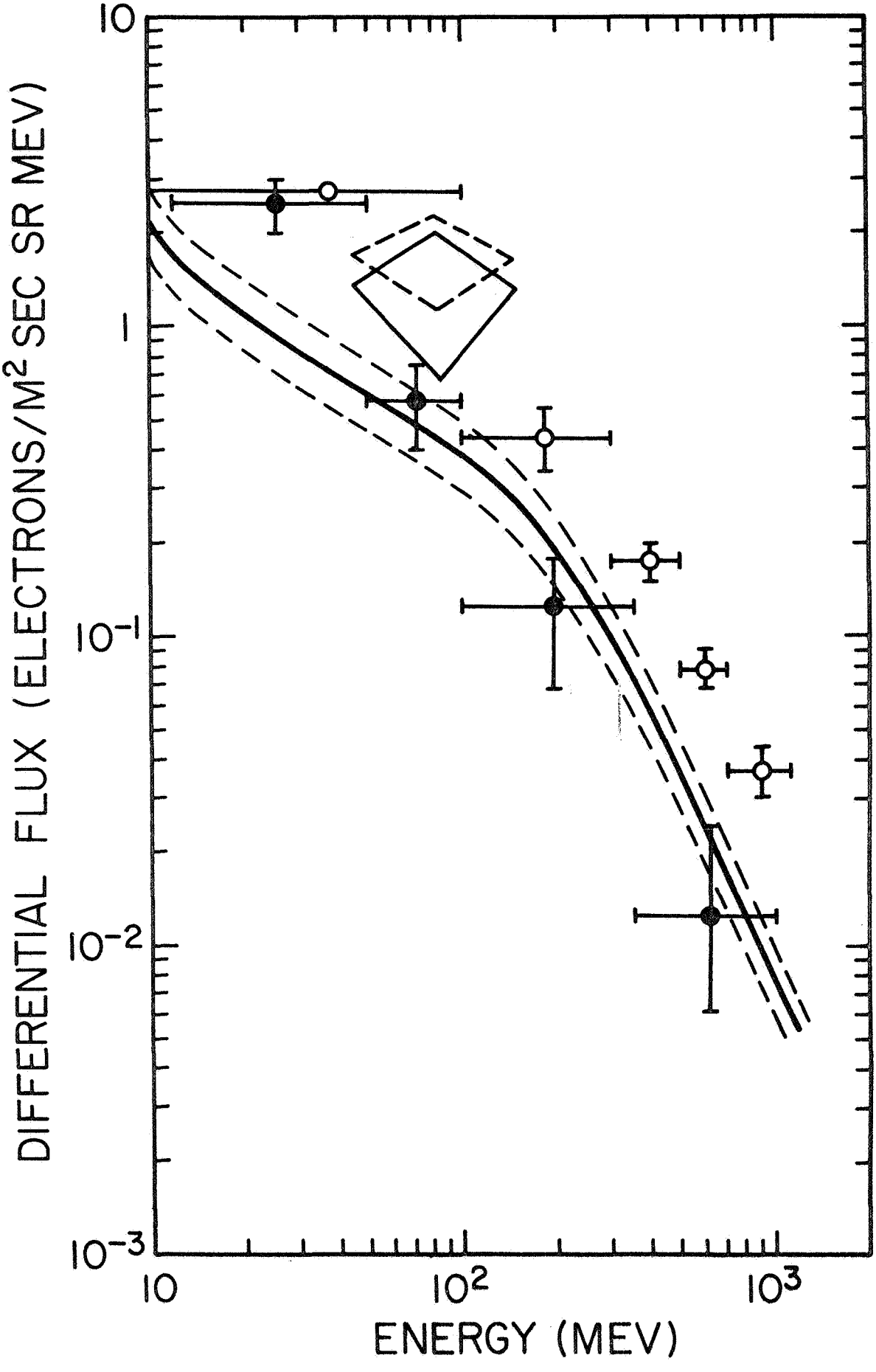
DIFFERENTIAL FLUX (ELECTRONS/M² SEC SR MEV)
10
1
10⁻¹
10⁻²
10⁻³
10
10²
10³
ENERGY (MEV)

Figure 7